ELSEVIER

Journal of Hazardous Materials B85 (2001) 273–290

Journal of Hazardous Materials

www.elsevier.com/locate/jhazmat

Estimation of the atmospheric corrosion on metal containers in industrial waste disposal

M. Baklouti [a,*], N. Midoux [a], F. Mazaudier [b], D. Feron [b]

[a] *Laboratoire des Sciences du Génie Chimique, CNRS–ENSIC, 1 rue Grandville, BP 451, F-54001 Nancy Cedex, France*

[b] *Commissariat à l'Energie Atomique–CEREM–Laboratoire d'Etude de la Corrosion Aqueuse, F-91191 Gif-Sur-Yvette Cedex, France*

Received 21 July 2000; received in revised form 13 April 2001; accepted 21 April 2001

Abstract

Solid industrial waste are often stored in metal containers filled with concrete, and placed in well-aerated warehouses. Depending on meteorological conditions, atmospheric corrosion can induce severe material damages to the metal casing, and this damage has to be predicted to achieve safe storage. This work provides a first estimation of the corrosivity of the local atmosphere adjacent to the walls of the container through a realistic modeling of heat transfer phenomena which was developed for this purpose. Subsequent simulations of condensation/evaporation of the water vapor in the atmosphere were carried out. Atmospheric corrosion rates and material losses are easily deduced. For handling realistic data and comparison, two different meteorological contexts were chosen: (1) an oceanic and damp atmosphere and (2) a drier storage location. Some conclusions were also made for the storage configuration in order to reduce the extent of corrosion phenomena.

Keywords: Heat transfer phenomena; Condensation modeling; Atmospheric corrosion; Industrial waste; Safety of storage

1. Introduction

Toxic wastes produced by industrial processes, e.g. nuclear or chemical processes, are often stored in metal containers which are placed either in aerated warehouses or in geological sites. The safety of such storage depends among other things, on the resistance of the metal containers to atmospheric corrosion.

* Corresponding author. Tel.: +33-3-83-17-51-74; fax: +33-3-83-17-53-26.
E-mail address: baklouti@ensic.u-nancy.fr (M. Baklouti).

0304-3894/01/$ – see front matter
PII: S0304-3894(01)00238-2

Nomenclature

Bi	Biot number ($=hL/k_s$)
C_i	corrosivity class (ISO 9223 Standard)
C_p	specific heat at constant pressure ($J\,kg^{-1}\,K^{-1}$)
$\bar{C}_p$	specific heat of the moist air ($J\,kg^{-1}\,K^{-1}$) ($=C_{p(\text{dry air})} + wC_{p(\text{vapor})}$)
$\mathcal{D}$	material diffusion coefficient ($m^2\,s^{-1}$)
e	equivalent thickness of condensed water (m)
g	acceleration of gravity ($m\,s^{-2}$)
Gr	Grashof number ($=\rho_f^2 g\beta\,\Delta TL^3/\mu_f^2$)
h	heat transfer coefficient ($=h_{lat}=h_{top}$, in Sections 5 and 6) ($W\,m^{-2}\,K^{-1}$)
h_{hum}	heat transfer coefficient in presence of water ($W\,m^{-2}\,K^{-1}$)
k	thermal conductivity ($W\,m^{-1}\,K^{-1}$)
k_m	mass transfer coefficient ($m\,s^{-1}$)
L	characteristic dimension (m)
Le	Lewis dimensionless number ($=Sc/Pr$)
L_v	latent heat of vaporization ($J\,kg^{-1}$)
$\dot{m}$	specific rate of phase-change ($kg\,m^{-2}\,s^{-1}$)
m_i	mass of condensed water on *unit-surface* i
M_{water}	molar weight of water ($=0.018\,kg\,mol^{-1}$)
M_{air}	molar weight of air ($=0.0288\,kg\,mol^{-1}$)
Nu	mean Nusselt number ($=hL/k_f$)
P	sulfur content of the atmosphere (represented by SO_2 deposition rate in $mg\,m^{-2}$ per day)
$\mathcal{P}$	atmospheric pressure (Pa)
Pr	Prandtl dimensionless number ($=C_{p,f}\mu_f/k_f$)
r	radial distance from the axis (m)
Ra	Rayleigh number ($=Gr\,Pr$)
S	Cl^- content of the atmosphere (represented by a deposition rate in $mg\,m^{-2}$ per day)
Sc	Schmidt number ($=\mu/\rho\mathcal{D}$)
t	time (s)
T	temperature (K)
T_m	mean temperature ($=(T_i + T_\infty)/2$) (K)
w	absolute humidity (kg vapor/kg dry air)
z	vertical distance from the floor (m)

Greek letters

β	thermal expansion coefficient (K^{-1})
ΔT	temperature difference ($=T_i - T_\infty$)
ε	relative humidity
ε_∞	ambient relative humidity
μ	dynamic viscosity ($Pa\,s^{-1}$)

ρ	density (kg m^{-3})
τ	wetness time (h per year)

Subscripts

f	relative to the fluid
floor	relative to the floor of the storage
i	at the interface
∞	ambient, far from the wall
lat	lateral
bot	affected to the bottom part of the container
top	affected to the top part of the container
L	relative to the liquid phase
s	relative to the solid (concrete)
v	relative to the vapor phase

The intensity of corrosion is generally considered to depend on the atmosphere humidity, the level of corrosive pollutants in air, and the nature of the solid surface of the container. In fact, the local intensity of corrosion on the container walls is also determined by the variations of the local humidity and the amount of water condensed on the solid surface. These variations depend not only on the meteorological but conditions also on the container's capacity in storing heat. Therefore this work was performed to study condensation and induced corrosion on the container walls, taking into account the ambient atmospheric conditions.

The first part of this work was devoted to the numerical modeling of heat and mass transfer, for two different meteorological conditions. This modeling allowed us to determine the variations of the local humidity and the amounts of water condensed on the solid surface. The corresponding atmospheric corrosion rate could be derived provided there was sufficient knowledge of the phenomena occurring on the solid surface. As a matter of fact, many additional parameters affect corrosion rates [1] depending on the nature and the thickness of the rust layer (see Section 6.3). Furthermore, no model is available for the quantitative description of corrosion phenomena at solids exposed to ambient air.

Hence, and this represents the second part of this work, the investigation was focused on obtaining a first estimation of the annual material loss of the various faces of the metal container, using the ISO/DIS 9223 Standard [2] which can be applied provided values of specific parameters such as the time of wetness (see Section 3.2). The originality of this work consists of replacing the usual ambient time of wetness relative to the outdoor meteorological conditions by a local evaluation of this wetness time characterizing the air layer at the surface of the container. This local "time of wetness" is determined by simulation of heat and mass transfer phenomena and is therefore more representative of the actual storage conditions. The final objective of the present work was to define the best storage conditions and to predict the corresponding duration of safe storage in actual conditions.

2. Investigation

For convenience, this investigation focused on the simple, but realistic, system of a vertical cylindrical steel container containing a solid waste; the waste materials were considered to be encased in inert concrete, as practiced for toxic materials. The whole system is placed in an aerated warehouse. Two configurations for storage were studied:

1. container standing on a concrete floor;
2. bottom-insulated system: such a situation is encountered when the container is installed on blocks, allowing an insulating air layer between the lower wall and the floor of the disposal room.

Since the investigation was designed to be representative of actual cases of waste storage, actual time variations of temperature and humidity of the ambient air to be used in the calculations, were obtained from the French meteorological office. Two different meteorological conditions were considered: (1) a very damp site, and (2) a warmer and dry location. In the following analysis, both studied cases will respectively be denoted as "the damp place" and "the dry place". Because of the discrete character of meteorological data, in terms of temperature and humidity level, we preferred to develop a home-made numerical code in which the data could be easily integrated. In addition, kinetic laws of corrosion phenomena will later be integrated in the code.

3. Modeling

Inside the container, the initial temperature is uniform, and heat transfer is purely conductive. The external transfers are supposed to lead to axial symmetry inside the container. Hence, Eq. (1) expresses heat conservation across a cylindrical *unit-volume* inside the container, for a two-dimensional geometry in the (r, z) plane

$$\rho C_p \frac{\partial T}{\partial t} = k \left(\frac{\partial^2 T}{\partial r^2} + \frac{1}{r} \frac{\partial T}{\partial r} + \frac{\partial^2 T}{\partial z^2} \right) \tag{1}$$

The thermal resistances inside the metal jacket at the lateral wall and on top are not taken into account as they are supposed very weak comparing to the external resistances of the boundary layers at those walls. In contrast, as far as the bottom part of the container is concerned, this resistance has been included in a global heat transfer coefficient (see Section 3.1).

In all cases, heat transfer between the bulk waste and the external air (or the floor) was supposed normal to the wall. Even if heat conduction through the metal covering along the remaining space direction should reduce temperature differences between the top and the bottom of the lateral surface, as well as those between the center and the periphery of the upper and lower parts of the container. This phenomenon is all the more pronounced as the metal jacket is thick. The comparison between some simulations taking into account wall thickness and others that neglect it establishes that results are quite similar for both cases making our assumption valid.

3.1. Boundary conditions

The stored material is placed in a warehouse in which the characteristics of the circulation of the ambient air has to be defined. Without precise information on the actual conditions of storage, different cases have therefore been worked for the different walls of the container. The boundary conditions on the various parts are given as follows.

- For the bottom of the container standing directly on the floor (configuration (a)), heat transfer is purely conductive across the steel lower wall and the very thin air layer comprised between the container and the floor and created by the roughness of the two media. Treatment for configuration (b) is similar, but with a different thickness for the isolating air layer. Corresponding contributions to heat transfer were estimated (see Section 5).
- For the lateral and the upper walls of the container,
    1. first, heat transfer at these walls was considered to be due to free convection, only, and the values used in the calculations might be underestimates of the actual transfer rates;
    2. the occurrence of artificial ventilation, or in contrast, of an isolated room were also investigated (see Section 5).

As far as modeling is concerned, classical linearization of the local heat flux in the boundary layer was used and global heat transfer coefficients h were introduced for this purpose.

In practice, for free convection, depending on the face considered, global or local heat transfer coefficients were used (see Section 3.3). For both other cases (e.g. artificial ventilation or isolation), the values of heat transfer coefficients are fixed and depend neither on time nor on the space co-ordinate. For the case of artificial ventilation, it must be remembered that heat transfer coefficients at the walls are expected to depend on the direction of the ventilation and the axial symmetry of the system is not preserved. Neglecting those aspects, we considered that ventilation induces a symmetric aeration on all the faces exposed to the circulating air.

3.2. Model assumptions and equations

Condensation and evaporation may be expected, depending on the ambient air humidity level, as well as on the temperatures in the air and at the wall surfaces. The following assumptions were made.

1. Preceding condensation, molecules of water adsorb on the metallic walls. This process involves an adsorption equilibrium. Consequently, heats of adsorption should be taken into account in the rigorous expression for the energy balance (Eq. (4)). However, this process was neglected for this first approach. By contrast, it was assumed in the model that corrosion can also occur during this period (see Section 3.2).
2. Condensation begins on the container surface as soon as the wall temperature T_i is below the dew temperature T_{dew} of the ambient air. The liquid–vapor equilibrium is assumed to establish instantaneously. Furthermore, it was postulated that condensed quantities of water were insignificant, so that the liquid film does not introduce any additional

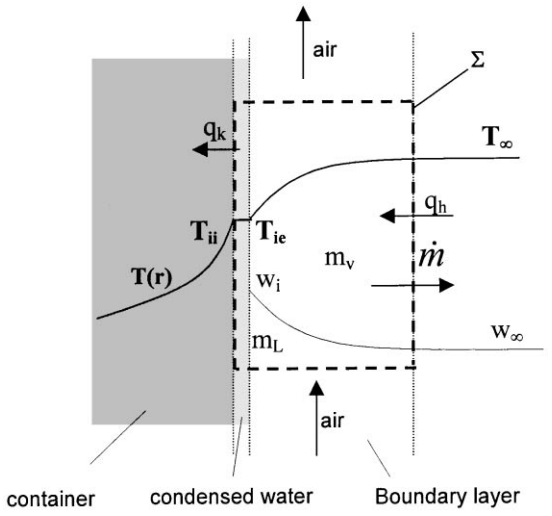

Fig. 1. Simplified representation of the storage in presence of condensation at lateral wall.

resistance to heat transfer at the walls. In practice, the wall temperature is the same as the one of the vapour–liquid interface: $T_i = T_{ii} = T_{ie}$ (see Fig. 1) and the interface can be considered as the part of the wall surface concerned with the phase change.

3. Hence, as long as liquid water is present on the wall, the absolute humidity w_i at the interface, that means characterizing the air just adjacent to the wall, is given by the saturation curve at the local temperature T_i.
4. Water condensation induces a gradient of vapor concentration at the wall, and subsequent vapor diffusion from ambient air to the wall surface. Hence, the specific mass flux of vaporization or condensation $\dot{m}$ is a function of the absolute moistures at the interface, w_i, and far from the wall, w_∞, and involves the apparent mass transfer coefficient k_m. When the sign of the local difference $(T_{dew} - T_i)$ changes, drying starts and takes place till the local amount of condensation m_i vanishes. This analysis leads to the following equations:

$$\dot{m} = 0, \quad \text{if } T_i > T_{dew} \quad \text{and} \quad m_i = 0 \quad \text{(no phase change)} \tag{2a}$$

$$\dot{m} = k_m(w_i - w_\infty), \quad \text{if } T_i > T_{dew} \quad \text{and} \quad m_i \neq 0 \quad \text{(evaporation)} \tag{2b}$$

$$\dot{m} = k_m(w_i - w_\infty), \quad \text{if } T_i \leq T_{dew} \quad \text{(condensation)} \tag{2c}$$

with the equilibrium constraint $w_i = w^s(T_i)$.

5. The model also considers that condensed water remains at the same location till its complete evaporation, which means that no water streaming on the container surfaces occurs.
6. State change involves additional heat: the heat released from condensation is utilized in warming the container materials and subsequent evaporation of the liquid water on the surface. Consider the system Σ including the boundary layer. The condensed water and

the walls (see Fig. 1), and for which S is the part of the surface normal to the heat and mass fluxes crossing Σ. Note that we assume that the mass and thermal boundary layers have the same thickness. Conservation of thermal energy in the system Σ leads to Eq. (4). In this balance, the air is not taken into account supposing that its enthalpy is invariant with temperature, and q_h and q_k are the convective and conductive heat fluxes counted positively. The amounts of liquid and gaseous water in the control volume delimited by Σ are, respectively, m_L and m_v and the enthalpy of water per unit-mass is designed as H_w.

$$\frac{d}{dt}(m_L H_w^L + m_v H_w^v) = q_h - q_k - \dot{m} S H_w^v(T_\infty) \tag{4}$$

Supposing steady-state for the vapor phase gives

$$\frac{d}{dt}(m_v H_w^v) = 0, \qquad \frac{d}{dt}(m_L H_w^L) = \dot{m} S H_w^L(T_i)$$

and hence Eq. (4) takes the form of

$$\dot{m}(C_{pw}^L(T_i - T^{ref}) + C_{pw}^v(T_\infty - T^{ref}) + L_v) = -h(T_i - T_\infty) - \lambda \left(\frac{\partial T}{\partial r}\right)_i \tag{5}$$

where L_v is the latent heat considered independent from temperature, T^{ref} a reference temperature, and C_{pw} is the specific heat of water. Neglecting both first terms in relation (5) and using (2b) or (2c), the heat balance reduces to

$$-\lambda \left(\frac{\partial T}{\partial r}\right)_i = k_m(w^s(T_i) - w(T_\infty))L_v + h(T_i - T_\infty) \tag{6}$$

The absolute moisture at saturation $w^s(T)$ can be calculated from the vapor pressure of water $P^s(T)$

$$w^s(T) = \frac{M_{water}}{M_{air}} \frac{P^s(T)}{\mathcal{P} - P^s(T)} \approx 0.6215 \frac{P^s(T)}{\mathcal{P} - P^s(T)} \tag{7}$$

where $\mathcal{P}$ stands for the atmospheric pressure (in Pa), and with the numerical law for P^s (T in °C)

$$P^s(T) = 610.78 \exp\left(\frac{17.269T}{T + 238.3}\right) \tag{8}$$

3.3. Modeling corrosion phenomena

Due to the presence of moisture and condensation, corrosion of the metallic walls of the container is likely to occur, strongly depending on the relative humidity at the interface ε_i (e.g. in the air just adjacent to the wall which is at temperature T_i). In addition, even if visible condensation occurs as soon as the relative humidity reaches 100%, single-layers of water molecules can cover the container walls before saturation [9]. As a consequence, atmospheric corrosion may occur generally for air humidity below saturation. For convenience, the arbitrary threshold value of $\varepsilon_i = 80\%$ was introduced [2] to assess the onset

of corrosion. In addition to the local relative humidity, the corrosion mechanism and rate are governed by other parameters. As a matter of fact, an important feature is the total time of wetness (in h per year), τ, i.e. with air relative humidity over 80%: τ thus represents the period per year in which corrosion is likely to occur. This time is of great interest for estimating material losses due to corrosion (see Section 6.3).

Wet–dry cycles constitute another important corrosion parameter as it seems that their number and their frequency are correlated to the atmospheric corrosion rate [1]. On each *unit-surface* of lateral and upper walls, a wet–dry cycle begins with a phase of dry state, is followed by a humid period, and ends as soon as the surface is dry again. Finally, it must be noted that the corrosion mechanisms differ one from another whether the surface is submitted to condensation or evaporation, or whether the surface is dry with $80\% < \varepsilon_i < 100\%$.

3.4. Heat and mass transfer coefficients

Correlations for heat transfer coefficients h due to natural convection were obtained from literature [3,4] for the various configurations investigated: (i) a lateral surface of a vertical cylinder, and horizontal surfaces oriented upward and (ii) being cooled or (iii) heated. They involve Rayleigh (Ra) and Nusselt (Nu) numbers, and coefficients C and n that are given in Table 1

$$Nu = C\,Ra^n \tag{9}$$

Using the physical properties of air involved in Eq. (9), the average heat transfer coefficients due to free convection can be calculated for the above configurations. The characteristic length appearing in Ra and Nu numbers is the height of the cylinder for case (i), and $0.9D$ for both cases (ii) and (iii) as recommended by White [4]. Calculations were made for a 2 m high cylinder with a diameter D of 1.5 m.

Rough estimates of heat transfer coefficients at the lateral and at the upper walls were obtained through preliminary calculations by varying the ambient temperature and the temperature gradient in the boundary layer. For gradients ranging from 0.5 to 5°C, the heat transfer coefficient is on the order of 1 W m^{-2} K^{-1}. The flow along the lateral wall changes

Table 1
McAdams correlations of average heat transfer coefficients using Eq. (9) and [4]

Case	Formula for global coefficients		Local heat transfer coefficients	
(i) Lateral	$10^4 < Ra < 10^9$	$C = 0.59, n = 14$	$10^4 < Ra < 10^9$	$Nu_z = 0.39Ra_z^{1/4}$
	$10^9 < Ra < 10^{13}$	$C = 0.13, n = 1/3$	$10^9 < Ra < 10^{13}$	$Nu_z = 0.12Ra_z^{1/3}$
(ii) Horizontal cooled	$10^5 < Ra < 2 \times 10^7$	$C = 0.54, n = 1/4$		
	$2 \times 10^7 < Ra < 3 \times 10^{10}$	$C = 0.14, n = 1/3$		
(iii) Horizontal heated	$3 \times 10^5 < Ra < 3 \times 10^{10}$	$C = 0.27, n = 1/4$		
	$3 \times 10^{10} < Ra < 10^{13}$	$C = 0.07, n = 1/3$		

from laminar to turbulent at temperature gradients over 2°C. Free convection over the upper surface was found to be mainly turbulent for a cooled surface and laminar for the last case of a heated surface.

Mass transfer coefficients were estimated from the heat transfer coefficients (h) using the Lewis number (Le) that compares thermal and mass diffusivities, through the Chilton–Colburn analogy [5,6]

$$\frac{h}{k_{\mathrm{m}}} = \bar{C}_p Le^{2/3} \tag{10}$$

4. Programme structure and resolution

On the walls of the container, each *unit-surface* of the mesh is described by its temperature T_{i} and the amount of water associated with this surface, m_{i}. The local state of the wall, characterized by the actual phenomena occurring on the surface, e.g. condensation, evaporation, stable dry surface, etc., represents another important property of the interface. Depending on this local state, the appropriate expression of $\dot{m}$ given by Eqs. (2a), (2b) and (2c) is used in the boundary condition (6).

Numerical integration of Eq. (1) coupled with Eqs. (2a)–(8) has been performed using the *finite-volume* method [7,8]. This method was chosen because of its physical significance and its performance in integrating such equations. An implicit first-order method with centered derivatives has been implemented in the numerical code. Since the momentum equation was not solved, no numerical diffusion could occur and the simple scheme used was sufficient for this work. Spatial and time discretization of the equations lead to a linear system which is solved by the Gauss–Seidel method [8]. The mesh size was uniform with computational steps at 0.01 m in the radial direction, and at 0.0285 m along the cylinder axis. As Eq. (6) is not linear, the expression of the absolute saturation moisture (7) was linearized using first-order Taylor approximation whereas the heat of vaporization was considered invariant with temperature. Typical time integration step was fixed at 30 s.

5. Simulations

A geometry representative of the actual containers was used with the dimensions given above. The thickness of the steel jacket was set at 10 mm and the waste material assumed to be similar to concrete having the following properties [10]: $k = 1.4\,\mathrm{W\,m^{-1}\,K^{-1}}$, $\rho = 2100\,\mathrm{kg\,m^{-3}}$, and $C_p = 900\,\mathrm{J\,kg^{-1}\,K^{-1}}$ in the temperature domain considered.

All the simulations presented here cover a 1-year period, from 1 January to 31 December; the initial temperature inside the container was fixed at 5°C. This temperature was chosen as it corresponds to a good approximation of the final temperature in the simulations performed.

Under free convection conditions at lateral and upper walls of the container, local heat transfer coefficients were calculated at the lateral wall (using Table 1), whereas for the upper surface, global coefficients were used (cases (ii) or (iii) of Table 1). In each case, heat transfer coefficients were recalculated at each step-time of the simulation.

Isolated and artificially ventilated storage were also simulated through respective values of $h = h_{lat} = h_{top} = 0.1$ and $h = 10\,W\,m^{-2}\,K^{-1}$: this investigation aimed at determining if additional ventilation or thermal insulation could hinder the rate of atmospheric corrosion on the walls.

Whatever the boundary conditions at the lateral and the upper walls, the global heat transfer coefficient at the bottom of the container, h_{bot}, was assumed to be $30\,W\,m^{-2}\,K^{-1}$ for the case (a) of a container standing on the floor, and (b) at $0.5\,W\,m^{-2}\,K^{-1}$ for the insulated configuration. These values were obtained considering the thermal resistances in series of the steel jacket 10 mm thick and the air layer between the container and the floor: the layer caused by the imperfect contact for the configuration (a) was assumed to be 1 mm thick, whereas a 50 mm layer was allowed by the presence of insulating blocks (configuration (b)).

The variations of the ambient temperature T_∞ and the relative humidity ε_∞ with time were supplied in the form of data files. In contrast, no data for the floor temperature T_{floor} were available. This temperature was then arbitrarily used for the model as follows: T_{floor} was constant at 8°C from 1 December to the 31 March, and at 18°C from 1 June to 30 September. Between June and September, it was taken at 18°C, and varied linearly with time between those periods. For one simulation, similar temperature profile but in the range 5–15°C was considered to assess the effect of T_{floor} on the simulation results.

6. Results

6.1. Validation of the model

The predicted amounts of condensed water were usually of low significance as detailed below, and the assumptions made in the condensation model were then validated. The time variations of the amount of condensate were calculated by the numerical code for each face of the cylinder. An equivalent water thickness (e) was deduced taking into account the water density and the face area.

Fig. 2 compares the water thickness on the vertical wall obtained for free convection for both of the studied meteorological situations studied. In all cases, the equivalent thickness is far less than 250 μm, and often below 50 μm. These calculated amount of condensed water enable one to consider a stagnant layer of water, with a coverage fraction of the wall far from unity: the water is to be retained on the wall surface and further evaporation allows cooling of the container. From a physical point of view, the model might be of dubious application for the highest condensate fluxes which should form rivulets at least as long as the surface is smooth, but such a situation is exceptional over the year, as shown in Fig. 2.

The other question to be addressed concerns the variation of the heat transfer coefficient in the presence of a significant quantity of water at the surface. In comparison to a dry surface situation with a corresponding heat transfer coefficient h, the actual coefficient in the presence of a liquid h_{hum} can be calculated from h and the thermal resistance due to the water film

$$\frac{1}{h_{hum}} = \frac{1}{h} + \frac{e}{k_{water}} \tag{11}$$

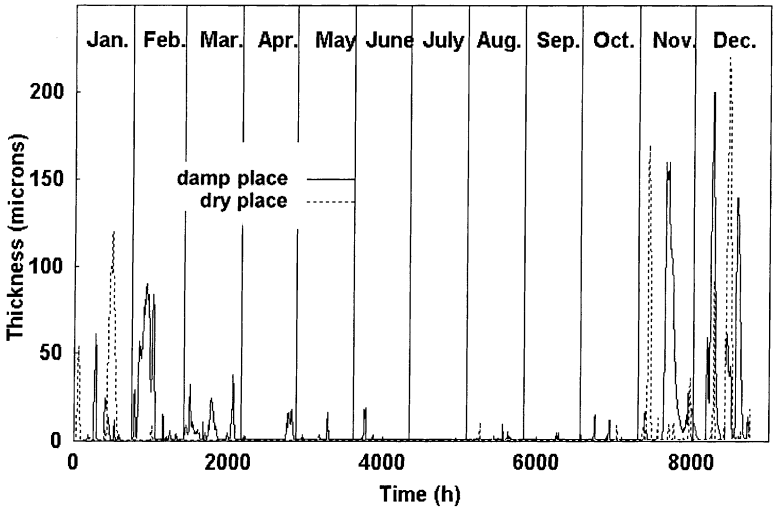

Fig. 2. Thickness of an equivalent film of water at lateral wall at the two disposal sites: free convection (h_{lat} and h_{top} calculated with relations of Table 1); bottom configuration (a).

Considering the maximum value of the film thickness (e), at 250 μm, and taking $k_{water} = 0.6\,W\,m^{-1}\,K^{-1}$ at ambient temperature, h_{hum} differs from h by only 5×10^{-2}%. This result validates the initial assumption of negligible effect of water condensation at the walls on heat transfer coefficients.

6.2. Heat and mass transfer coefficients

Fig. 3 shows the time variations of the heat transfer coefficient at the lateral surface and the upper wall for the two sites under free convection conditions (using relations from Table 1). For the lateral wall, as local heat transfer coefficients were handled during simulation, the global values which are reported in Fig. 3 result from averaging local values over the vertical abscissa.

After a short transient period, heat transfer coefficients remain fairly constant with time with the following orders of magnitude: $h_{lat} = 1.7$ and $1.5\,W\,m^{-2}\,K^{-1}$, $h_{top} = 1.2$ and $1.1\,W\,m^{-2}\,K^{-1}$, for the dry and the humid locations, respectively. Mass transfer coefficients on the container walls calculated using the Chilton–Colburn analogy, are then subject to weak variations with time, a result which constitutes an important piece of information for storage operation.

Since the thermal conductivity inside the container remains constant, the effect of heat transfer coefficient at the walls and of Biot number Bi at the same surface, are identical.

6.3. Corrosion rate estimation

Different approaches can be considered for the assessment of atmospheric corrosion. First, a phenomenological approach would consist in applying for each time step of the

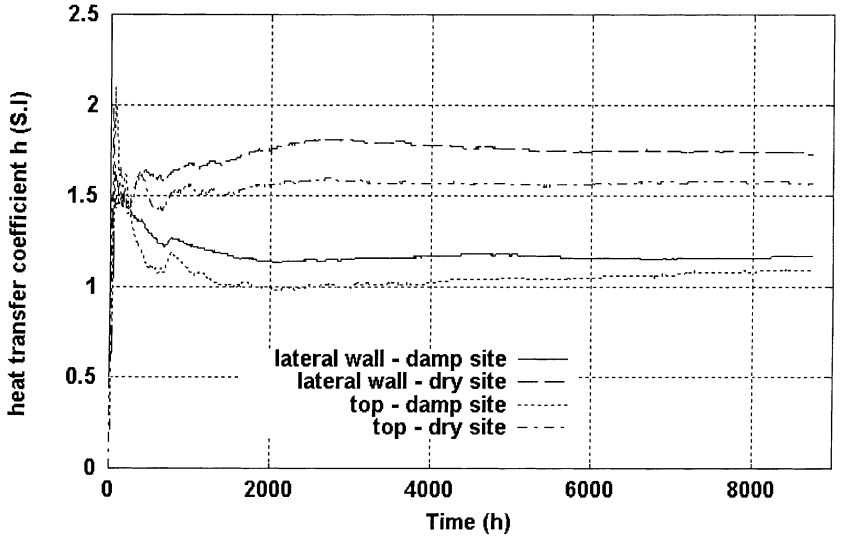

Fig. 3. Time evolution of free convection heat and mass transfer coefficients at lateral and superior walls with both meteorological contexts (bottom configuration (a)).

simulation, the appropriate atmospheric corrosion kinetics. Nevertheless, this approach requires accurate knowledge of the electrochemical mechanisms, which is not straightforward since wetting and drying corrosion phenomena are different processes [1]. Moreover, the complexity is increased by the change in morphology of the rust layer for the different phases of the wet–dry cycle. Experiments are now in progress, and are to allow significant gain in knowledge in this area, with a better understanding of the processes involved. While waiting for the results of the work undertaken in the field, it was preferred to use a more global approach relying upon the classes of corrosivity C_1 to C_5 defined by the ISO 9223 Standard [2]. In terms of corrosion rate, each class is related to a material loss after 1 year of exposure. Table 2 gives the corresponding losses for common metals.

According to the ISO 9223 Standard [2], the class of atmospheric corrosivity C_i depends on various atmospheric parameters among which (1) τ_∞: the ambient time of wetness, (2) S: the airborne salinity represented by the deposition rate (mg m^{-2} per day) of chloride ion,

Table 2
Corrosion rates (μm per year) on the well-defined metal panels of the various classes of corrosivity given by the ISO 9223 Standard [2]

Classes of corrosivity C_i	Steel	Zinc	Copper	Aluminum
C_1 (very weak)	0.1–1.3	<0.1	<0.1	Negligible
C_2 (weak)	1.3–25	0.1–0.7	0.1–0.6	<0.25
C_3 (medium)	25–51	0.7–2	0.6–1.3	0.25–0.8
C_4 (high)	51–83	2–4.2	1.3–2.8	0.8–2
C_5 (very high)	>83	>4.2	>2.8	>2

Table 3
Correspondence between classes of pollution and concentrations of atmospheric pollutants represented by deposition rates [2]

Class	Sulfur dioxide		Chlorides	
	Deposition rate ($mg\,m^{-2}$ per day)	Examples ($mg\,m^{-2}$ per day)	Class	Deposition rate
P_0	<10	Countryside, non polluted areas	S_0	<3
P_1	10–35	Countryside, little polluted areas	S_1	3–60
P_2	35–80	Industrial areas	S_2	60–300
P_3	80–200	Industrial and highly polluted areas	S_3	300–900

and (3) P: the sulfur-containing compounds content represented by deposition rate of the sulfur dioxide SO_2 ($mg\,m^{-2}$ per day). The correspondence between C_i and the values for (τ_∞, S, P) can be found in the relevant literature [2,11].

The wetness time in ambient air τ_∞ only depends on meteorological conditions and atmospheric pollution whereas the local wetness time in the vicinity of the container also depends on the thermal inertia of the storage as well as on heat and mass transfer at walls. A local time of wetness has be associated with each face of the container. Note that in our numerical code, τ is an average of the local values obtained in the vicinity of each *unit-surface* of the mesh. It should be noted that in the same way, all the global variables presented here, result from local evaluations and subsequent averaging over the considered area.

Hence, knowing the values of S and P, and determining the value of τ by simulation, the corrosivity class of the "local" or indoor air, i.e. in the vicinity of the storage, can be determined. This class may differ from the corrosivity class of the ambient (i.e. outdoor) air that can be determined directly from parameters τ_∞, S and P and without any simulation.

Because of the lack of reliable values for airborne salinity and sulfur content in the storage sites considered, two extreme couples of values (S_0, P_0) and (S_3, P_3) were tested for the two sites. The corresponding air pollution concentrations given in Table 3.

First, it can be noted from the results reported in Tables 4 and 5 that the ambient wetness time τ_∞ is in all cases greater than the actual wetness time of the storage, τ. This fact

Table 4
τ (day per year) in the *damp site* (year 97) on the two exposed walls and for different h values

Nature of the heat transfer at walls	Heat transfer coefficients ($W\,m^{-2}\,K^{-1}$)	Biot number (lateral wall)	Bottom configuration	τ at lateral wall	τ at superior wall	τ_∞
Isolated	$h = h_{lat} = h_{top} = 0.1$	5.4×10^{-2}	Floor (a)	216	231	
Free convection	$h_{lat} \cong 1.2 - h_{top} \cong 1.1$[a]	0.64	Floor (a)	238	252	
Free convection[b]	$h_{lat} \cong 1.2 - h_{top} \cong 1.1$	0.64	Floor (a)	261	279	
Free convection	$h_{lat} \cong 1.2 - h_{top} \cong 1.1$[a]	0.64	On blocks (b)	254	255	
Forced convection	$h = h_{lat} = h_{top} = 10$	5.4	Floor (a)	254	260	
–	–	–	–	–	–	266

[a] Values obtained from Fig. 3.

[b] Those values correspond to a different couple of floor temperature: T_{floor} is in the range [5; 15°C] for a specific case or in the range [8; 18°C] for the rest.

Table 5
τ (day per year) in the *dry site* (year 97) on the two exposed walls and for different h values

Nature of the heat transfer at walls	Heat transfer coefficients ($W\,m^{-2}\,K^{-1}$)	Bottom configuration	τ at lateral wall	τ at upper wall	τ_∞
Isolated	$h = h_{lat} = h_{top} = 0.1$	Floor (a)	97	100	
Free convection	$h_{lat} \cong 1.7 - h_{top} \cong 1.5$[a]	Floor (a)	86	95	
Free convection	$h_{lat} \cong 1.7 - h_{top} \cong 1.5$[a]	On blocks (b)	88	95	
Forced convection	$h = h_{lat} = h_{top} = 1$	Floor (a)	92	95	
–	–	–	–	–	152

[a] Values obtained from Fig. 3.

particularly notable for the drier site, meaning that meteorological conditions lead to overestimates of the wetness time. The results also show the significant influence of ventilation on the calculated time of wetness relative to each wall (Tables 4 and 5).

Considering lower values of T_{floor} between 5 and 15°C, results in higher condensation flux, as expected. However, the wetness time are changed only to a minor extent (~10%) by this parameter (Table 4) and the various trends observed with T_{floor} in the range 8–18°C remain valid.

Another important parameter is the ambient relative humidity averaged over the year $\bar{\varepsilon}_\infty$. In the damp site, $\bar{\varepsilon}_\infty$ attains 85%, whereas this value is around 69% for the dry site. Indeed, this parameter can be helpful in understanding the different behaviors observed for both sites: as shown in Fig. 4, for disposal in the damp site, τ tends to τ_∞ as h (or Bi) increases. This result can be interpreted as follows: for high values of Bi, heat transfer is controlled by thermal diffusion inside the container, and the temperature gradient at the wall is very low

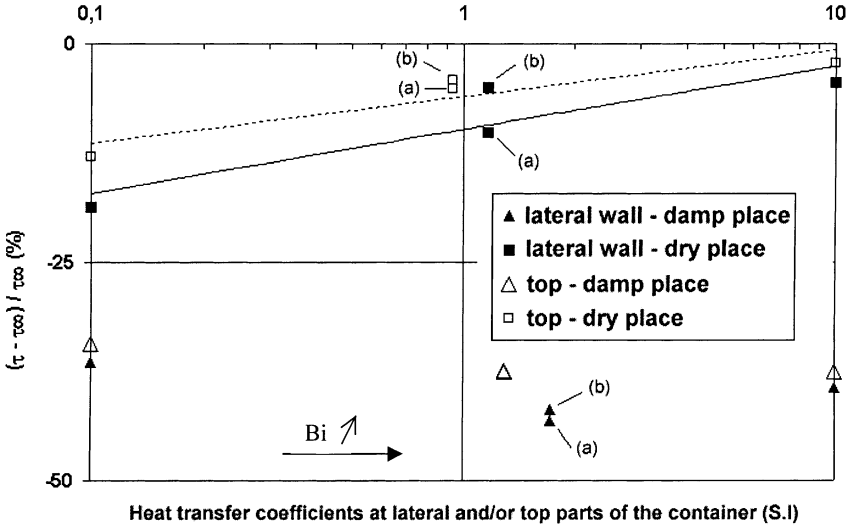

Fig. 4. Comparison between local and ambient wetness times for both meteorological situations and with various air circulation and configurations (a) floor and (b) on blocks.

Table 6
Corrosivity classes at the lateral wall and far from the walls for extreme values S and P (damp place)

h (W m^{-2} K^{-1})	Bottom configuration	Classes of airborne salinity S and sulfur content P in the atmosphere	
		$S_0/S_1 - P_0/P_1$	$S_3 - P_3$
0.1	Floor	C_3	C_5
Free convection	Floor	C_4	C_5
Free convection[a]	Floor	C_4	C_5
Free convection	On blocks	C_4	C_5
10	Floor	C_4	C_5
External conditions	–	$C_\infty = C_4$	$C_\infty = C_5$

[a] Those values correspond to a different couple of floor temperature: T_{floor} is in the range [5; 15°C] for a specific case or in the range [8; 18°C] for the rest.

in comparison with the gradient inside the container. Thus, mean relative humidity $\bar{\varepsilon}_i$ and wetness time τ, both related to the actual storage conditions, tend to their corresponding values only defined on meteorological conditions $\bar{\varepsilon}_\infty$ and τ_∞. On the other hand, in the warmer location where the mean relative humidity is quite lower, the local time of wetness passes through a minimum for middle-range values of *Bi* (Fig. 4). In case which $\varepsilon_\infty < 80\%$, an important temperature gradient in the boundary layer ($T_i \ll T_\infty$) is required to allow ε_i to exceed 80%: this situation may occur for low values of *Bi*. Nevertheless, this gradient will remain all the more that the temperature inside the container is noticeably below the wall temperature, corresponding to great *Bi* values. Hence, middle-range Biot numbers can correspond to the shortest wetness times and then offer the best situations in regards to corrosion for the dry site whereas it corresponds to low Biot values for the damp place.

Comparing both meteorological situations, it is also useful to notice that for the humid place, ambient and local times of wetness differ from <25%, while in the dry place, this difference can reach values close from 50%. Considering local times of wetness rather than ambient times for assessment of atmosphere corrosion, will then contribute to a better estimation of the actual corrosion damage.

Considering lower values of T_{floor} between 5 and 15°C results in higher condensation flux, as expected. However, the wetness time are changed only to a minor extent (∼10%) by this parameter (Table 4) and the various trends observed with T_{floor} in the range 8–18°C remain valid.

These results are of more practical interest when expressed in terms of corrosivity of the atmosphere for the different sites and boundary conditions. Large wetness times correspond to classes of high corrosivity that are related to high atmospheric corrosion rates given in Table 2. Although the τ values determined for the lateral wall and the upper face differ one from another, the corrosion rates at the two surfaces correspond to the same corrosivity class which is reported in Tables 6 and 7, depending on boundary and meteorological conditions. Comparison of those Tables show that, for similar pollution of atmosphere and similar boundary conditions, safer storage conditions are offered by the drier location, at least for low values of airborne salinity and sulfur contents. Note that for steel and according to Table 2, $C_{2/3}$ corresponds to material losses around 30 μm per year, whereas C_5 is over 83 μm per year.

Table 7
Corrosivity classes at the lateral wall and far from the walls for extreme values S and P (dry place)

h (W m^{-2} K^{-1})	Bottom configureation	Classes of airborne salinity S and sulfur content P in the atmosphere	
		$S_0/S_1 - P_0/P_1$	$S_3 - P_3$
0.1	Floor	C_3	C_5
Free convection	Floor	$C_{2/3}$	C_5
Free convection	On blocks	$C_{2/3}$	C_5
10	Floor	$C_{2/3}$	C_5
External conditions	–	$C_\infty = C_3$	$C_\infty = C_5$

Moreover, if for high levels of pollution (S_3, P_3) the corrosivity of the atmosphere remains constant, the climate and the boundary conditions have an influence on corrosion rate for low pollutant concentrations. It can be noted that this dependence is not the same for both storage locations: increasing air circulation increases corrosion in the damp site, but reduces this phenomena in the drier site (Tables 6 and 7). This result shows the importance of simulation for prediction of storage safety, as the intensity of corrosion seems largely dependent, among other things, on the meteorological conditions, and cannot thus be derived from general extrapolations. As far as the configuration of the bottom part of the container is concerned, no significant differences are observed.

Hence, it clearly appears that a better prediction of corrosion rates will rely first on the modeling of corrosion phenomena. In addition, before considering a more accurate modeling of heat transfer at the metal jacket, simple measurements of the actual ambient

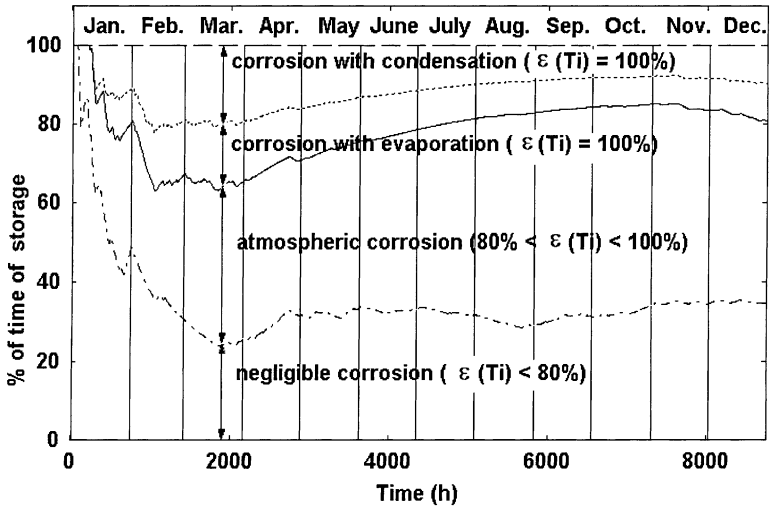

Fig. 5. Time proportions of the different phases encountered during one year of storage at the lateral wall at the damp place. Boundary conditions: free convection (h_{lat} and h_{top} from Table 1); bottom configuration (a).

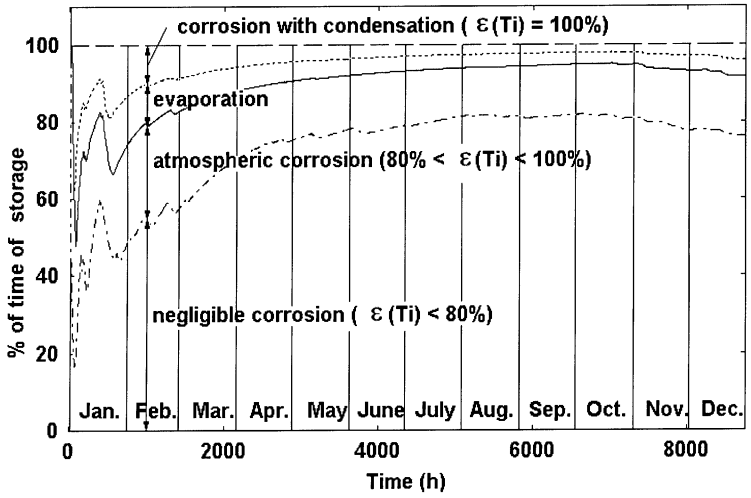

Fig. 6. Time proportions of the different phases encountered during one year of storage at the lateral wall at the dry place. Boundary conditions: free convection (h_{lat} and h_{top} from Table 1); bottom configuration (a).

air concentrations of sulfur dioxide and chloride ions at the vicinity of the storage container should allow to obtain closer assessment of the actual atmosphere corrosivity.

Figs. 5 and 6 clearly show that the time fraction of evaporation and condensation are of the same order. This result may be expected as mass transfer coefficients show moderate deviations over the year (see Fig. 3 and Eq. (10)) and since it is assumed that no water streaming occurs. Both processes then occur during periods that mainly depend on the absolute moisture gradient in the material boundary layer. Figs. 5 and 6 also show that lower fractions are observed for wetted surfaces, i.e. for $80\% < \varepsilon < 100\%$ in the damper site, and for predominance of dry surface, with $\varepsilon < 80\%$, in the other site. Again, this difference is due to the mean humidity over the year which is greater than 80% at the more humid site but under 70% in the drier location. Consequently, although none of phenomena discussed can be neglected, it appears that the occurrence of atmospheric corrosion in the absence of water represents a significant contribution of the observed corrosion rates. This information is very valuable in the elaboration of models for corrosion kinetics.

Again, the comparison of the two storage sites shows that the dry site offers safer storage conditions, with larger periods of negligible corrosion than in the more humid location.

7. Conclusions

This paper describes a model of the thermal behavior of a cylindrical container suitable for storage of inert waste, and condensation rates in terms of duration of corrosion periods and amounts of water on walls can be estimated. A comparative study was performed for two different climates; from all points of view, the drier disposal with reduced humidity is better protected from corrosion than the damp site. We also observed that heat and mass transfer coefficients are fairly constant over the year, and that the storage procedure —

canister standing on the floor or insulating blocks — has a moderate impact only, on the significance of corrosion phenomena. The characteristics required for estimation of the corrosion rates can be successfully yielded by the simulation.

Hence, a macroscopic method for estimation of the range of corroded thickness per year — with the results of experimental measurements of the ambient temperature, humidity, and the contents of chloride and sulfur species, as well as the floor temperature on the site — has been elaborated. Important conclusions can be deduced from this first approach, concerning both the influence of the various parameters involved, and the directions to future work for model refinement and prediction of the local corrosion rates.

Furthermore, preliminary experiments (data not shown) reveal that the duration of the last phase of drying of the wet–dry cycle, as well as the number of wet–dry cycles over the year play an important role in the structure of the superficial rust layer of the steel covering. Both parameters can be calculated with the model presented.

Further work will consist in testing other conditions of annual humidity to establish possible correlation between meteorological conditions and the corrosion rate. Besides, corrosion modeling will be improved by implementing empirical corrosion kinetics in the model. These involve the corroded thickness per year $\mathrm{Ep_c}$, the time of exposure τ, and empirical coefficients k_c and n_c under the form

$$\mathrm{Ep_c} = k_c t^{n_c} \tag{12}$$

where coefficients k_c and n_c depend on the considered site and can be determined from corrosion measurements. Later, the heat transfer model will be applied to the prediction of corrosion rates by integrating corrosion models of physical meaning in wet–dry cycles.

Finally, the behavior of a stack of cylindrical containers, as done under storage practice should be modeled using the existing model of a single container.

Acknowledgements

Thanks are due to Dr. F. Lapicque for assistance in preparation of the manuscript.

References

[1] D. Landolt, Corrosion et chimie des surfaces des métaux, in: Traité des Matériaux, Vol. 12, Presses Polytechniques & Universitaires Romandes, Lausanne, 1993.
[2] French ISO/DIS 9223 Standard, Metals and Alloys Corrosion — Classification of Corrosivity of Atmospheres, ANFOR, 1989.
[3] F.P. Incropera, D.P. De Witt, Fundamentals of Heat and Mass Transfer, 3rd Edition, Wiley, New York, 1990.
[4] F.M. White, Heat Transfer, Addison-Wesley, New York, 1984.
[5] F. Kreith, M.S. Bohn, Principles of Heat Transfer, Harper and Row, New York, 1986.
[6] N. Midoux, Mécanique et Rhéologie des Fluides en Génie Chimique, Tec et Doc. Lavoisier, Paris, 1988.
[7] S.V. Patankar, Numerical Heat Transfer and Fluid Flow, McGraw-Hill, New York, 1980.
[8] J.H. Ferziger, M. Peric, Computational Methods for Fluid Dynamics, 2nd Edition, Springer, Berlin, 1999.
[9] C. Leygraf, Corrosion Mechanisms in Theory and Practice, Marcel Dekker, New York, 1995.
[10] W.M. Rohsenow, J.P. Hartnett, L.Y. Cho, Handbook of Heat Transfer, 3rd Edition, McGraw-Hill, New York.
[11] L. Vrobel, D. Knoktova, Using the Classification of corrosivity of atmospheres to extend the service life materials, structures and products, in: S.W. Dean, T.S. Lee (Eds.), The Degradation of Metals in the Atmosphere, ASTM STP 965, 1988.